Intercomparison of gamma scattering, gammatography, and radiography techniques for mild steel nonuniform corrosion detection

Article *in* The Review of scientific instruments · March 2011

DOI: 10.1063/1.3562893 · Source: PubMed

CITATIONS
26

READS
335

8 authors, including:

Priyada Panikkath
Alagappa University
33 PUBLICATIONS **152** CITATIONS
SEE PROFILE

M. Margret
Indira Gandhi Centre for Atomic Research
8 PUBLICATIONS **81** CITATIONS
SEE PROFILE

Ramar R
Indira Gandhi Centre for Atomic Research
10 PUBLICATIONS **90** CITATIONS
SEE PROFILE

Shiva Ramu
Indira Gandhi Centre for Atomic Research
28 PUBLICATIONS **414** CITATIONS
SEE PROFILE

Intercomparison of gamma scattering, gammatography, and radiography techniques for mild steel nonuniform corrosion detection

P. Priyada,[1,a)] M. Margret,[1] R. Ramar,[1] Shivaramu,[1] M. Menaka,[2] L. Thilagam,[3] B. Venkataraman,[1,2] and Baldev Raj[4]
[1]*Radiological Safety Division, Indira Gandhi Centre for Atomic Research, Kalpakkam-603 102, Tamil Nadu, India*
[2]*Quality Assurance Division, Indira Gandhi Centre for Atomic Research, Kalpakkam-603 102, Tamil Nadu, India*
[3]*Atomic Energy Regulatory Board Safety Research Institute, Kalpakkam-603 102, Tamil Nadu, India*
[4]*Indira Gandhi Centre for Atomic Research, Kalpakkam-603 102, Tamil Nadu, India*

(Received 25 December 2010; accepted 10 February 2011; published online 18 March 2011)

This paper focuses on the mild steel (MS) corrosion detection and intercomparison of results obtained by gamma scattering, gammatography, and radiography techniques. The gamma scattering non-destructive evaluation (NDE) method utilizes scattered gamma radiation for the detection of corrosion, and the scattering experimental setup is an indigenously designed automated personal computer (PC) controlled scanning system consisting of computerized numerical control (CNC) controlled six-axis source detector system and four-axis job positioning system. The system has been successfully used to quantify the magnitude of corrosion and the thickness profile of a MS plate with nonuniform corrosion, and the results are correlated with those obtained from the conventional gammatography and radiography imaging measurements. A simple and straightforward reconstruction algorithm to reconstruct the densities of the objects under investigation and an unambiguous interpretation of the signal as a function of material density at any point of the thick object being inspected is described. In this simple and straightforward method the density of the target need not be known and only the knowledge of the target material's mass attenuation coefficients (composition) for the incident and scattered energies is enough to reconstruct the density of the each voxel of the specimen being studied. The Monte Carlo (MC) numerical simulation of the phenomena is done using the Monte Carlo N-Particle Transport Code (MCNP) and the quantitative estimates of the values of signal-to-noise ratio for different percentages of MS corrosion derived from these simulations are presented and the spectra are compared with the experimental data. The gammatography experiments are carried out using the same PC controlled scanning system in a narrow beam, good geometry setup, and the thickness loss is estimated from the measured transmitted intensity. Radiography of the MS plates is carried out using 160 kV x-ray machine. The digitized radiographs with a resolution of 50 μm are processed for the detection of corrosion damage in five different locations. The thickness losses due to the corrosion of the MS plate obtained by gamma scattering method are compared with those values obtained by gammatography and radiography techniques. The percentage thickness loss estimated at different positions of the corroded MS plate varies from 17.78 to 27.0, from 18.9 to 24.28, and from 18.9 to 24.28 by gamma scattering, gammatography, and radiography techniques, respectively. Overall, these results are consistent and in line with each other. © *2011 American Institute of Physics*. [doi:10.1063/1.3562893]

I. INTRODUCTION

Corrosion is one of the most major problems in infrastructure maintenance and responsible, in part, for deterioration of capital-intensive systems, such as bridges, buildings, nuclear power plant concrete structures, pipelines, storage tanks, aircraft ships, cars, trucks, and machinery. Therefore, it is important not only to be able to detect but also to measure the extent of metal loss accurately due to corrosion. A wide range of NDE techniques have been reported in the literature that may be suitably employed for the monitoring of corrosion of steel for the purpose of diagnosing the cause and extent of the corrosion. Many of the technologies of NDE/non-destructive testing (NDT) lend themselves to the detection, characterization, and quantification of corrosion damage, and generally, the method for corrosion detection depends on the reduced thickness of the component following corrosive attack. This is normally the underlying concept for corrosion detection by NDT methods such as radiography, ultrasonic, and eddy currents. No single means of corrosion detection is either ideal or suitable for all forms of corrosion. There are major advantages and disadvantages of the primary corrosion detection and characterization technologies as well as the corrosion mechanism they used to detect.

The need for advanced techniques for detection and evaluation of embedded corrosion and a class of subsurface defects that require access only to the one side of any material or structure relatively thick to be inspected has drawn

a)Author to whom correspondence should be addressed. Electronic mail: priyada@igcar.gov.in. Fax: +9144-27480235.

attention to the x-ray or gamma backscatter as a desirable choice.[1–4] Compton scattering measurements have been employed in the past for industrial applications to detect inhomogeneity, voids, and cracks at the interior of not accessible structures or to determine density or density variations.[5–7] The same technique has been applied to the problem of identifying and detecting explosive material in airport luggage and buried land mines.[8–10] Compared to transmission or gammatography technique, scattering technique requires more scanning time and the reconstruction procedure is tedious. Even then it is accepted for more precise and point information from single sided accessible targets.

The most common sources today are the x-ray photon sources, which provide low energy photons. Soft x rays generated by high voltage, miniaturized x-ray tubes may be turned off at will, pose little radiation exposure risk to operating personnel. The x rays from an electrically operated device are not as penetrating as gamma radiation since x rays typically have lower photon energies than gamma rays. The sample thickness is limited by the low penetrability of the primary x-ray beams. The disadvantage of using the radioactive isotopes is the low counting rate compared to the high counting rate by using x rays. On the other hand, the gamma rays from radioactive isotopes produce an energy spectrum that has distinct emission energy peaks, thus providing well-defined photon energies that enable easier analysis of the measured signal. Moreover, gamma ray isotopic sources are readily portable, self-contained, self-energizing, and usable in hostile environments. Instead of low energy photons, one can use bremsstrahlung photon beams (3–6 MeV) from small electron linear accelerator (LINAC) for greater penetrability and high intensity. These unique features make it a very desirable for industrial based applications. Despite the clear technological and practical advantages of LINACs over radioactive sources, the latter still occupy an important place in application armamentarium, mainly, because of considerably lower capital, installation and maintenance costs of these radioactive sources compared to LINACs. The other advantages of these radioactive sources are relatively long half-life, high specific activity, and simple means of production. It is very convenient to use ^{137}Cs radioactive source which emits photons of energy 661.6 keV, within the energy range where the Compton process dominates. The ^{60}Co (1.17 and 1.33 MeV) can also be used for higher penetration but it is desirable to use radioisotopes that emit mostly at a single energy, otherwise detector may not be able to distinguish between scattered energies of the original photons with energies very close to each other and an ambiguity arises and the variation of count rate with energy and density becomes much more complex.

The concept of gamma scattering method is based on the detection of scattered radiation produced from a collimated beam aimed at the object. The measurements can be drawn from relatively small volume, which makes it feasible for point to point scanning. This method is a viable tool for inspecting material since it is an interaction, which is strongly dependent on the electron density of the scattering medium and in turn on its mass density. Therefore, the information obtained by this technique is strongly related to the material density, thus allowing changes in the material uniformity to be monitored. The material density is obtained from point to point, and it is not necessarily complex mathematical models which determine the density of the test object. Gamma or x rays scattered from a well-defined volume element (voxel) are detected by a well-collimated detector placed at an angle which could vary from forward scattering angles to the backscattering configuration. The choice of scattering angle used is then dictated by the energy of the incident photons. The reflected signal provides a measure of the electron density, ρ_e, of the material comprising the inspected volume. By scanning a well-defined volume element through a plane of interest in an object, using a raster motion, it is possible to obtain density distribution in this plane. In this process each recorded signal comes from a different depth, and in this way, it is possible to get information about the density profile. This approach can be widely applied, e.g., for nondestructive material examination in industry and aviation, detection of landmines and explosives, and investigating the constitution of archeological artifacts. Hence, gamma scattering enables the detection of local defects and the discrimination between materials of different density and composition. Despite its possible applications Compton scattering is not widely used. This is mainly due to the longer time which is required for a complete scan compared to transmission method, but another reason is that the reconstruction problem is far more specific to the geometry of the experimental apparatus.[11–17] This is essentially due to the absorption of gamma rays inside the object. Unlike transmission data, however, data obtained by scattering method are nonlinear due to attenuation of the incident and scattered photons in the material surrounding each scatter site. In fact, while in transmission method the absorption constitutes the quantity to be measured, in scattering method it represents a source of artifacts.[11] The reconstruction algorithm should correct for absorption inside the sample.

This paper focuses on the mild steel (MS) corrosion detection and intercomparison of results obtained by gamma scattering, gammatography, and radiography techniques. A simple and straightforward reconstruction algorithm to reconstruct the densities of the objects under investigation and an unambiguous interpretation of the signal as a function of material density at any point of the thick object being inspected is described. In this method the density of the target need not be known and only the knowledge of the target material's mass attenuation coefficients (composition) for the incident and scattered energies is enough to reconstruct the density of the each voxel of the specimen being studied. As the scattered intensity depends on the effective density and thickness of the sample within the voxel, the magnitude of corrosion and average loss in thickness within the voxel are determined by iteration from the known values of mass attenuation coefficients and the geometrical parameters. The loss in thickness due to corrosion is compared with those values obtained from the transmission and radiography techniques.

II. EXPERIMENTAL PROCEDURE

The scattering experimental setup shown in Fig. 1 is an automated PC controlled scanning system consisting of CNC controlled six-axis source detector system

FIG. 1. (Color online) The gamma scattering scanning system.

and a four-axis job positioning system. The collimated and lead shielded ^{137}Cs radioactive source of activity 155.4 GBq (4.2 Ci) and a 50% efficiency coaxial high-purity germanium (HPGe) detector providing high resolution energy dispersive analysis of the scattered spectrum are mounted separately on the source and detector sub-assemblies of six-axis system. The motion of the specimen disk is derived by four servo motors, three motors used to move it in three perpendiculars Cartesian coordinate system denoted XYZ. One more servo motor is used to rotate it and this coordinate is denoted by W. The servo motors are controlled by Galil's DMC 2040 motion controller programmed with Galil's commands and the commands are communicated from PC via high speed RS 232 port. The positional accuracy of the source and detector system is ± 50 μm for X- and Z-axis travel stages and for four-axis job positioning system it is $\pm 10\mu$m for X-, Y-, and Z-axis travel stages. The positional accuracy for θ rotary stages for both the systems is $\pm 0.25^{\circ}$.

The gamma spectroscopic data acquisition is done by FAST COM 8K Multi Channel Analyzer (MCA) PC Add-on card. The translation, rotation, and vertical motions of four-axis CNC controlled job position system and MCA data acquisition are fully automated using Visual Basic (VB) based windows application program. The data acquisition, parameter setting of the MCA, and the four-axis motion are automated using dynamic link library and Galil's Active-x tool files. The PC first sends the signal to digital motor controller (DMC) to reset the position by energizing the servo motors and then it will direct the MCA to collect the data in preset live time. Many different tasks can be executed by simple commands such as initialization, position sensing, repositioning the scanner, start and stop a measurement, store the accumulated data on disk, and automatically execute all steps for a complete sequential scanning. The collected counts in the specified energy region are stored in the output file of PC. The output file contains parameters of collection time, scanning period, X and Z positions, angle, gross, and net photo counts for the given region of interest.

Two MS flat plates, one normal and another corroded of dimensions $0.235 \times 0.155 \times 0.01$ m^3, are chosen for corrosion detection and quantification. They are placed at a distance of 0.845 m from the source and the detector's distance from the plates is 0.337 m with the angle of scattering 113°. The voxel to be analyzed is geometrically established by the intersection of the incident and scattered beams, as defined by the input and output collimators of source and detector, respectively, and depends on size of the collimators employed and on the source–structure, detector–structure distances and can be easily chosen by proper adjustment of X, Y, Z, and θ positions of six-axis and four-axis job positioning systems. The diameter of both the source and detector collimators is 0.007 m and the resulting voxel is 17.618×10^{-6} m^3. The incident photon energy emitted by ^{137}Cs is 661.6 keV and the energy of the scattered photon is 243 keV. The scattered intensity from the specified voxel of the MS flat plates is detected using HPGe detector and the pulse-height spectrum (PHS) is accumulated. The scattered spectra are recorded with the number of channels nearly equal to 2000 and each channel width is 0.205 keV.

The gammatography experiments are carried out using the same PC controlled scanning system in a narrow beam, good geometry setup and the thickness loss is estimated from the measured transmitted intensities. The radiography of the MS plates is carried out using Balteu 160 kV x-ray machine. The digitized radiographs with a resolution of 50 μm are processed for the detection of corrosion damage in four different locations. Optical density of the film will vary with the change in thickness for a particular material which is radiographed, and the calibrated values with known thickness variation are taken as input for determination of corrosion damage at the unknown location.

III. GAMMA SCATTERING TECHNIQUE AND AN ALGORITHM FOR RECONSTRUCTION OF THE OBJECT'S DENSITY

A simple and straightforward reconstruction algorithm to reconstruct the object's density and an unambiguous interpretation of the signal I (P) as a function of material density at any point of the object being inspected is given here. Using this algorithm the densities of the normal and corroded regions of the MS flat plates can be reconstructed directly from the scattered intensities. The schematic diagram of backscatter geometry of the experimental arrangement is shown in Fig. 2. For simplicity, we will assume that the photons from

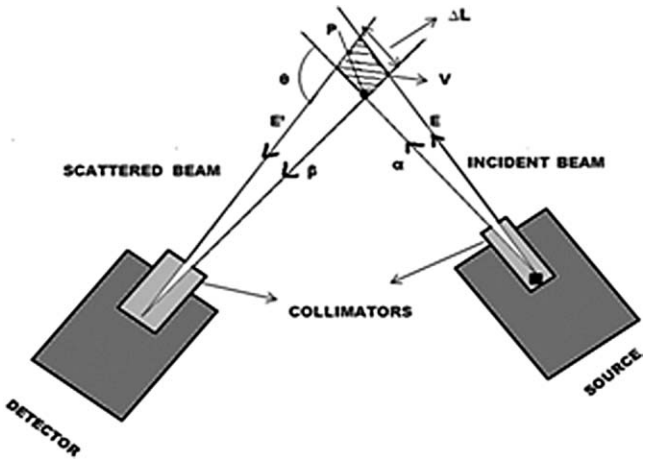

FIG. 2. Schematics of the backscattering geometry.

the source undergo only one scattering. We will also ignore the small attenuation by the air between the object and the backscatter system.

The number of detected photons depends on the number of scattered photons as well as on the attenuation all along the path within the material. The path of photons from the source to the detector can be divided into three stages which determine their contribution to the measured signal. The first stage is the photons travel from the source to the scattering point P along path α. In a homogeneous material gamma rays are attenuated according to the Beer–Boucher law

$$I_1 = I_0 \exp - \left[\left(\frac{\mu\,(E_0)}{\rho}\right)\rho x\right], \tag{1}$$

where I_1 and I_o are the transmitted and incident fluxes, respectively, $\mu\,(E_0)/\rho$ is the mass attenuation coefficient of the material for photons of energy E_0, ρ is the density of the material, and x is the length of path α. The second stage of development for our signal is the scattering toward the detector which occurs at point P. The scattered flux, I_2, is determined by

$$I_2 = I_1 \frac{d\sigma\,(E_0, \Omega)}{d\Omega} S\,(E_0, \theta, Z)\, d\Omega \rho_e V, \tag{2}$$

where $d\sigma\,(E_0, \Omega)/d\Omega$ is the differential scatter cross section as governed by the Klein–Nishina formula, S is the incoherent scattering function (a function of the incident gamma energy E_0, the scatter angle, θ, and atomic number of the element), $d\Omega$ is the solid angle subtended by the detector and its collimator, V is voxel volume (product of source beam area A_s and voxel thickness ΔL along α) and $\rho_e(P)$ is the electron density at point P. The electron density at P is the material property we are attempting to measure. It is proportional to the physical density ρ according to the formula

$$\rho_e = \rho N \frac{Z}{A}, \tag{3}$$

where N is Avogadro's number, Z is the atomic number, and A is the atomic weight. The detected spectrum is complicated by two effects. The first one is due to the preferential removal of photons from a specific spectral region due to the absorption in the sample and the second one is due to the generation of secondary radiation due to multiple interactions. The third stage of development is the transport of the scattered photons back through the materials toward the detector. The signal is further attenuated, so that

$$I_3 = I_2 \exp - \left[\left(\frac{\mu\,(E)}{\rho}\rho x'\right)\right], \tag{4}$$

where I_3 represents the flux intensity reaching the detector, $\mu(E)/\rho$ is the mass attenuation coefficient for scattered photons of energy E, now a function of θ by the virtue of the Compton energy shift at P, and x' is the length of path β. Combining the expressions for the three stages, the signal intensity corresponding to point P can be written as

$$I\,(P) = I_0 \exp - \left[\left(\frac{\mu\,(E_0)}{\rho}\right)\rho x\right] \frac{d\sigma\,(E_0, \Omega)}{d\Omega} S\,(E_0, \theta, Z) \times d\Omega \rho_e(P) V \exp - \left[\left(\frac{\mu\,(E)}{\rho}\right)\rho x'\right]. \tag{5}$$

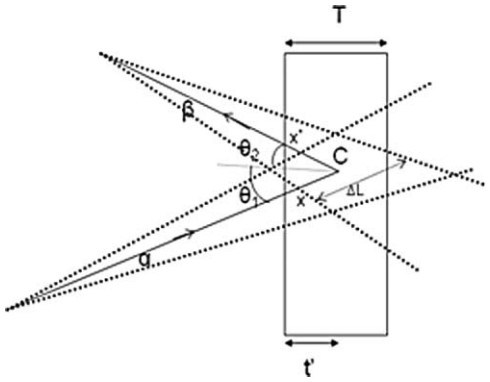

FIG. 3. The geometry for calculating the attenuation factor.

According to Eq. (5) we can expect an unambiguous interpretation of the signal I(P) as a function of material density at point P. Nonhomogeneous materials (or those with irregular surfaces) present a different problem. In these cases μ becomes a function of position, which requires that the attenuation terms be integrated over the path lengths involved.

The geometry for calculating the attenuation factor (AF) for the voxel is shown in Fig. 3. Let C be the point in the center of the voxel and t' be the corresponding thickness of the MS flat plate at which scattering takes place. Then for this case the incident and scattered paths are given by $x = t'/\cos(\theta_1)$ and $x' = t'/\cos(\theta_2)$, respectively.

The AF is given by

$$AF = \int_0^T \exp - \left\{\left(\frac{\mu\,(E_0)}{\rho}\right)\rho \frac{t'}{\cos(\theta_1)} + \left(\frac{\mu\,(E)}{\rho}\right)\rho \frac{t'}{\cos(\theta_2)}\right\} dt', \tag{6}$$

$$= \frac{\left[1 - \exp - \left\{\left(\frac{\mu(E_0)}{\rho}\right)\sec(\theta_1) + \left(\frac{\mu(E)}{\rho}\right)\sec(\theta_2)\right\}\rho T\right]}{\left(\left(\frac{\mu(E_0)}{\rho}\right)\sec(\theta_1) + \left(\frac{\mu(E)}{\rho}\right)\sec(\theta_2)\right)\rho}. \tag{7}$$

By incorporating Eq. (7) in Eq. (5) signal intensity at point P is

$$I\,(P) = k\rho AF, \tag{8}$$

where

$$k = \frac{d\sigma\,(E_0, \Omega)}{d\Omega} S(E_0, \theta, \Omega)\, d\Omega A_s N \frac{Z}{A}. \tag{9}$$

Average thickness of voxel for corroded plate can be determined by taking the ratios of I(P) of corroded to normal.

In gamma scattering investigations, the information concerning the object structure is provided by the single scattered component of the detected radiation. Secondary scatter events occur when the scattered photons from the primary interactions interact again before leaving the object. When the detector receives photons from these secondary events, another form of superposition artifact can be produced. The multiple scatter components contribute a background signal which reduces detail and contrast. Corrections for the effects of multiple scattering are essential for improving the sensitiv-

ity, accuracy, and prediction. In the idealized system the detector collimator can be expected to exclude most secondary scatter. These multiple interactions may be due to multiple scattering, multiple photoelectric interaction, or mixture of scattering/photoelectric interaction. Multiple scattering events may derive from collisions within the volume element itself or alternatively from collisions outside this volume and these events enhance the intensity of the whole spectrum. The contribution of multiple scattering to the overall detector signal depends on the type of material and the energy of primary radiation. The probability of a multiple interaction depends on the terms of the absorption coefficients of the sample matrix and on the size of the interaction volume. The multiple interaction contribution to the spectrum can be considered negligible when the absorption of radiation is small, and the probability of a multiple interaction depends on the number of photons that are generated in a sample by interactions producing secondary photons. In this case multiple interaction and self-absorption are interconnected, but they produce opposite effects on the spectrum. The effect of the multiple scattered radiation on the quality of the reconstructed density can be expressed in terms of the multiple scatter fraction (MSF) defined by

$$\mathrm{MSF} = \frac{\mathrm{N_m}}{\mathrm{N_m}+\mathrm{N_s}}, \tag{10}$$

where $\mathrm{N_s}$ and $\mathrm{N_m}$ are, respectively, the single and multiple scattered photon fluences detected by the detector. MSF increases with scattering angle and as expected, also with ΔE, with the thickness of the scattering object, and with the atomic number of the material.

Some attempts to solve the problem analytically have been made, which can be found from the literature,[18,19] but must be considered to be very crude approximations, partly because they do not include an energy distribution. Multiple scattering can be evaluated with the MC method. Many interesting results of MC calculations have been reported, especially, by the groups interested in the development of new devices for the measurement of the Compton profile.[20,21] The results reported show that the energy distribution of the multiple scattered photons is quite flat and that the contribution can be considered negligible when a light matrix and a small sample have been used. The solution to multiple scattering is to use a high energy resolution detector so that multiple scattering contribution can be separated and setting smaller energy window width ΔE around the Compton peak and is followed in the present investigation. The Compton scattering process has however a unique characteristic, in that both the intensity and scattered photon energy have direct dependence on the choice of scattering angle. With a suitable choice of source, detector, and spectrometer geometry the intensity of multiple scattering can be reduced to a tolerable level, providing only a relatively flat background to the scattering signal.

IV. MONTE CARLO CALCULATIONS

The MC simulations have been done which takes into account the detailed characteristics of the source, detector, and the scatterer in calculating the PHS. The MCNP4C (Ref. 22) radiation transport code is applied to perform the calculations in this work and it is a general purpose, three-dimensional general geometry, time-dependent code, which is used to calculate coupled neutron–photon–electron transport in bulk media. For photons, the code accounts for incoherent and coherent scattering, the possibility of fluorescent emission after photoelectric absorption, absorption in pair production with local emission of annihilation radiation, and bremsstrahlung. MCNP provides a nearly predictive capability of how radiation interacts with matter. In MCNP simulations, each particle (photon) is tracked from creation until termination with all interactions based on physics models and cross sections, and all decisions (location of interaction, scattering angle, etc.) are based on pseudorandom numbers. Usually, the results of a simulation are normalized per starting source photon. New source photons are randomly created until a preset number of histories are tracked and the simulation is ended.

The desired result in the simulation component of this study is a PHS since it produces the distribution of the energy deposited in a "cell," i.e., the gamma ray energy spectrum in a physical model of a detector. The PHS simulations are implemented in MCNP in the so-called "f8 tally." This estimator is based on the following fundamental approaches: (i) the energy bins in gamma ray spectra simulations correspond to the energy deposited in the detector cell summed over all the tracks of a history; (ii) no integral is evaluated, but the deposited energy in a cell is calculated based on the detailed microscopic radiation tracking; and (iii) if the photon does not undergo interactions in a specified cell, no energy is deposited and the photon does not contribute to the PHS. Hence, for each history, only one count is added to the spectrum. The pulse height tally is used to obtain the energy distribution of pulses created in the volume of the germanium crystal. The f8 energy bins correspond to the total energy deposited in a detector in the specified channels by each physical particle. Thus, the detector geometry is modeled with the MCNP code, which simulates the detection process to obtain the spectral shape. To obtain a good representation of the experimental spectra, a standard MCNP Gaussian broadening of the pulse-height response is used to define the full width at half maximum (FWHM) of the crystal and is given by

$$\mathrm{FWHM\,(MeV)} = \mathrm{a} + \mathrm{b}\sqrt{(\mathrm{E} + \mathrm{cE}^2)}. \tag{11}$$

Here a, b, and c are constants and E is the energy of the photon in mega-electron-volt.

Two ^{137}Cs radioactive source capsules, each of activity 77.7 GBq (total 155.4 GBq), are deposited inside stainless steel capsule and the HPGe detector is modeled with the surrounding lead shielding and a 0.007 m beam collimator for both source and detector. The HPGe detector consists of a crystal of size 0.066 m $\times$ 0.066 m surrounded and sealed by an aluminum layer 0.002 m thick in front and 0.001 m on sides. The dimensions of the MS flat plates and their distances from the collimator edge of the source and detector setup, the size of the collimators, and the angle of scattering are incorporated in to the modeling. The MC PHS contains 135 bins, each with a width of 2.08 keV and the photon energies ranged from 27 to 310 keV. The measured PHS is rebinned to the

same energy grid as the MCNP calculation for the purpose of comparison. For the pulse-height (energy-deposition) estimates used in this study, the source biasing represents the only feasible method to improve computational efficiency. Herewith, the directional (source) biasing function is used to make the source emitting particles to move as a fine beam toward the MS flat plates. Two different MCNP simulations are carried out to study the normal and corroded MS flat plates. Each simulation is run with 2.1×10^9 source particles. This number of source particles is chosen because the absolute efficiency value approaches a steady value and the relative variance decreases as the number of source particle increases. The calculated spectrum is normalized to the experimental ones absolutely by multiplying the number of photons emitted by ^{137}Cs source during a time interval for which the experimental PHS is recorded. To do this, the values of the simulated PHS are multiplied by a factor (source activity $\times$ acquisition time of the experimental spectrum) which allowed direct comparison with the experimental spectrum corrected for background or the experimental data are divided by the same factors to compare with the MCNP simulated PHS.

V. RESULTS AND DISCUSSION

The experimental scattered PHS is plotted as a function of energy for the normal and corroded MS flat plates and is shown in Fig. 4. The gamma scattered photopeak intensity from corroded MS flat plate decreases up to 11.41% for the same size voxel compared to a normal MS flat plate and this corresponds to an average thickness loss of 0.027 m due to corrosion in a MS flat plate of size $0.235 \times 0.155 \times 0.01$ m^3. This can be explained based on the following reasoning. As the sensitive volume intersects the corroded MS flat plate, there is a reduction in the volume of the material in the voxel due to loss in thickness and hence the total electron density and, therefore, a decrease in the detector response. The average thickness in the different voxels of corroded MS flat plate are reconstructed from the corresponding experimental scattered intensities using the reconstruction algorithm described in Sec. III. The voxel position and its size are calculated from the size of the collimators and source–sample and sample–detector distances. The μ/ρ and μ'/ρ are computed using the XCOM program which can generate photon cross sections for scattering, photoelectric absorption, and pair production as well as total attenuation coefficients, for any element, compound, or mixture (atomic number $\leq$100), at energies from 1 keV to 100 GeV.[23]

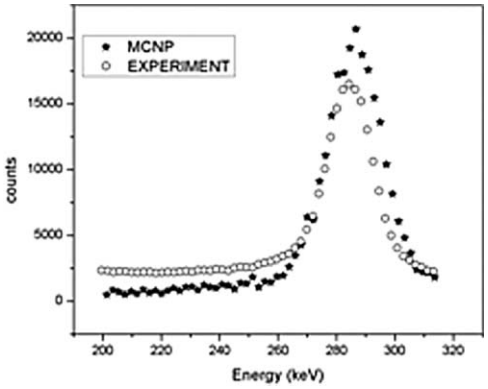

FIG. 5. The comparison of MC simulated scattered spectra with experimental results.

The result of MCNP PHS simulations and the comparison of the spectral shape with the experimental ones are shown in Fig. 5. A good agreement in the shape of the PHS is seen between the experimental spectra and those of the MC simulated ones. Thus measurements support the MC simulations. In field conditions one will be looking for corroded structures with density losses varying from few percent onward. The MC simulation of MS flat plate corrosion varying from the present case of 6.6% extending up to 60% is done. The photopeaks of the simulated scattered spectra are shown in Fig. 6 and the quantitative estimates of the values of signal-to-noise (S/N) ratio from these spectra, i.e., the ratios of count rate of normal MS flat plate to corroded one, are plotted as

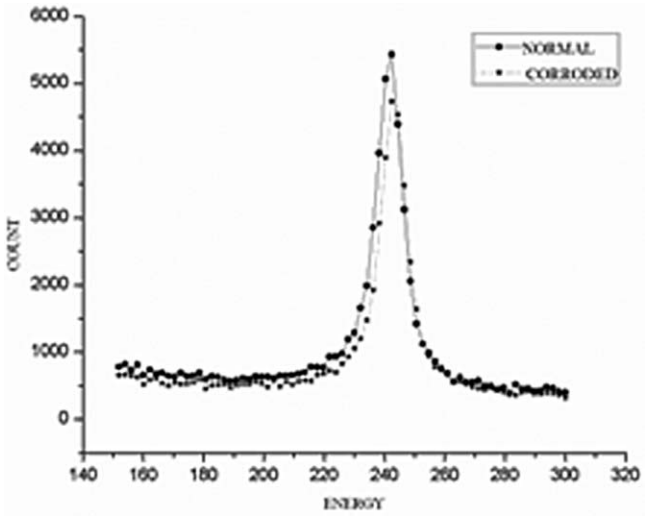

FIG. 4. The experimental scattered PHS plotted for the normal and corroded MS plates.

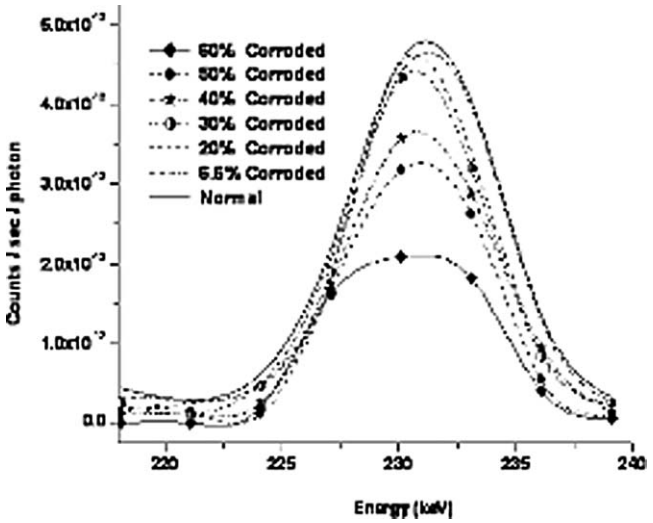

FIG. 6. The MC simulated scattered spectra for corroded MS flat plate for various percentage of corrosion.

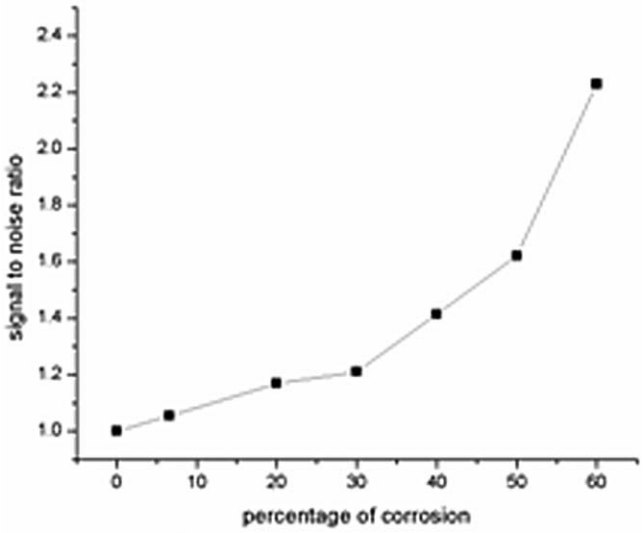

FIG. 7. The quantitative estimates of the values of S/N plotted as a function of the percentage of the MS flat plate corrosion.

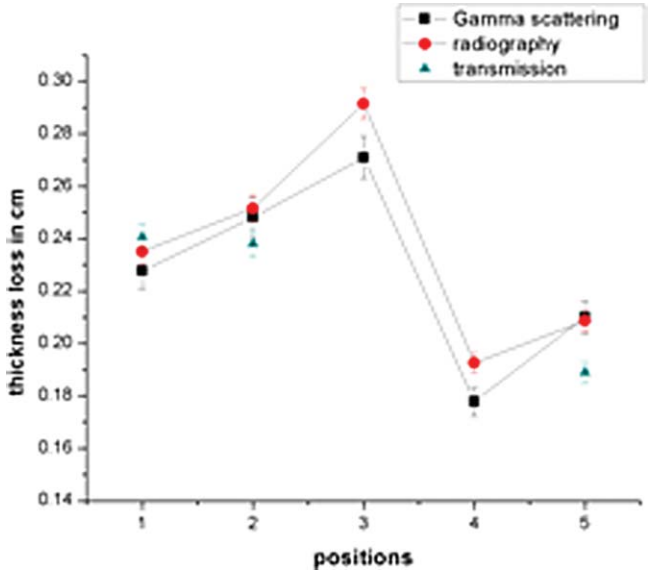

FIG. 9. (Color online) Measured thickness loss by gamma scattering, radiography, and gammatography techniques.

a function of the percentage of corrosion and are shown in Fig. 7. The S/N values vary from 1.054 (6.6% corrosion) to 2.229 (60% corrosion).

Figure 8 shows the radiographic images of the reference and corroded plates. It is observed from the radiographic image [Fig. 8(a)] that corrosion damage initialization has occurred in the reference plate also. Corrosion at five different locations of corroded MS plate is evaluated using the known calibrated values. The loss in thicknesses due to corrosion measured by gamma scattering method is compared with those values obtained from the gammatography and radiography techniques and are shown in Fig. 9. The error on measured thickness loss by gammatography, scattering, and radiography is 2%, 3%, and 2%, respectively. The percentage thickness loss estimated at different positions of the corroded MS plate varies from 17.78 to 27.0 by gamma scattering, from 18.9 to 24.28 by gammatography, and from 19.26 to 29.15 by radiography method. Overall, these results are consistent and in line with each other.

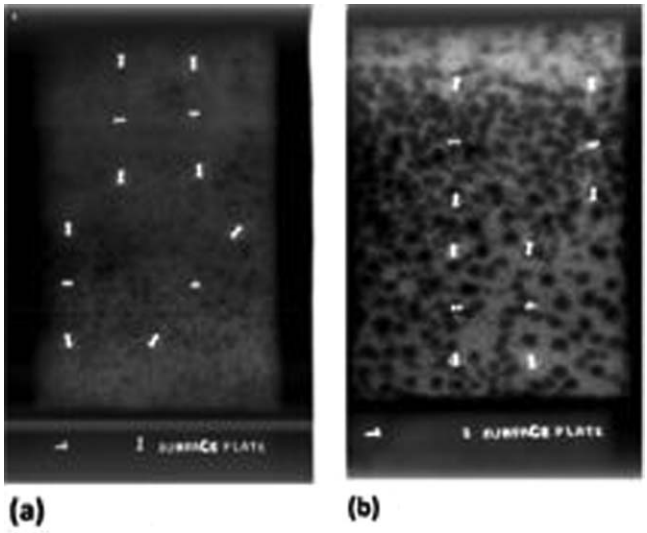

FIG. 8. Radiography images of the (a) normal (b) corroded MS plates.

VI. CONCLUSIONS

An intercomparison of results obtained by gamma scattering, gammatography, and radiography method is reported. An automated gamma scattering scanning system and a technique for corrosion detection, quantification, and evaluation that require access only to the one side of any material or structure relatively thick to be inspected are described. A simple and straightforward reconstruction algorithm to reconstruct the densities of the objects under investigation and an unambiguous interpretation of the signal as a function of material density at any point of the thick object being inspected is described. The percentage thickness loss estimated at different positions of the corroded MS plate varies from 17.78 to 27.0, from 18.9 to 24.28, and from 18.9 to 24.28 by gamma scattering, gammatography, and radiography techniques, respectively. Overall these results are consistent and in line with each other. The MC numerical simulation of the phenomena is done using the MCNP code, and the quantitative estimates of the values of S/N ratio of the MS flat plate corrosion varying from 6.6% extending up to 60% are calculated to get an indication of the magnitude of S/N one can get in this type of investigations and the PHS spectra are compared with experimental ones. The measurements support the MC simulations. The experimental and MC simulation results show that the scattering method is highly sensitive to changes in the electronic and physical densities of the volume element under study, and the magnitude of embedded corrosion can be clearly identified and quantified by monitoring single scattered events. The main advantage of the scattering method as compared to other techniques is the ability to detect and quantify corrosion in any material or structures without the need for all-round access to the structures under investigation and it is also possible to inspect a chosen volume or point.

The photon scattering is preferable to other forms of NDE in certain cases: high contrast even for thick samples, good spatial resolution, three-dimensional capability, and the ability to make direct real-time density measurements of only the volume of interest within the sample.

ACKNOWLEDGMENTS

The support of DAE research fellowship to P. Priyada is gratefully acknowledged. The first four authors thank Dr. N. Mohankumar, Head, RTAS, RSD, IGCAR, for his constant support and encouragement.

[1]K. Banerjee and W. L. Dunn, Appl. Radiat. Isot. **65**, 176 (2007).
[2]L. R. Lawson, Mater. Eval. **60**, 1295 (2002).
[3]G. Harding, Radiat. Phys. Chem. **50**, 91 (1997).
[4]E. M. A. Hussein and T. M. Whynot, Nucl. Instrum. Methods Phys. Res. A **283**, 100 (1989).
[5]B. Achmad and E. M. A. Hussein, Appl. Radiat. Isot. **60**, 805 (2004).
[6]A. Tartari, G. Maino, E. Lodi, and C. Bonifazzi, Radiat. Phys. Chem. **61**, 737 (2001).
[7]N. Adil, Br. J. Non-Destr. Test. **19**, 72 (1977).
[8]S. Yuk, K. H. Kim, and Y. Yun, Nucl. Instrum. Methods Phys. Res. A **568**, 388 (2006).
[9]E. M. A. Hussein, M. Desrosiers, and E. J. Waller, Radiat. Phys. Chem. **73**, 7 (2005).
[10]G. Harding, Radiat. Phys. Chem. **71**, 869 (2004).
[11]B. Golosio, A. Brunetti, and R. Cesareo, Nucl. Instrum. Methods Phys. Res. B **213**, 108 (2004).
[12]N. V. Arendtsz and E. M. A. Hussein, IEEE Trans. Nucl. Sci. **42**, 2155 (1995).
[13]S. J. Norton, J. Appl. Phys. **76**, 2007 (1994).
[14]F. A. Balogun and N. M. Spyrou, Nucl. Instrum. Methods Phys. Res. B **83**, 533 (1993).
[15]J. P. Hogan, R. A. Gonsalves, and A. Krieger, IEEE Trans. Nucl. Sci. **NS-587 38**, 1721 (1991).
[16]R. Cesareo and S. Mascarenhas, Nucl. Instrum. Methods Phys. Res. A **277**, 669 (1989).
[17]G. Harding and R. Tischler, Phys. Med. Biol. **31**, 477 (1986).
[18]J. Sherman, Spectrochim. Acta **7**, 283 (1955).
[19]T. Shiraiwa and N. Fujino, Jpn. J. Appl. Phys. **5**, 886 (1966).
[20]R. L. Clark and G. Van Dyk, Phys. Med. Biol. **18**, 532 (1973).
[21]C. E. Webber and T. J. Kennett, Phys. Med. Biol. **21**, 760 (1976).
[22]*MCNP™, a general Monte Carlo n-particle transport code*, version 4C LA-13709-M, edited by J. F. Briesmeister (Los Alamos National Laboratory, NM, 2000).
[23]M. J. Berger and J. H. Hubbel, XCOM: Photon Cross Sections Database, Web Version 1.2, available at http://physics.nist.gov/xcom. National Institute of Standards and Technology, Gaithersburg, MD 20899, USA (1999). Originally published as NBSIR 87-3597, "XCOM: Photo cross sections on a personal computer," (1987).